Emergence of a fluctuating state in the stuffed tridymite-type oxides $Ba_{1-x}Sr_xAl_2O_4$

Y. Ishii,[1,*] H. Tsukasaki,[1] E. Tanaka,[1] S. Kawaguchi,[2] and S. Mori[1]

[1]*Department of Materials Science, Osaka Prefecture University, Sakai, Osaka 599-8531, Japan*

[2]*Japan Synchrotron Radiation Research Institute (JASRI), SPring-8, Sayo, Hyogo 679-5198, Japan*

(Received 12 June 2016; revised manuscript received 26 August 2016; published 11 November 2016)

We investigated the crystal structures and dielectric properties of an improper ferroelectric $Ba_{1-x}Sr_xAl_2O_4$ ($x \leqslant 0.1$) and revealed that suppressing the condensation of the M-point soft mode involves the emergence of a "fluctuating" state. In the low-Sr-concentration region of $x \leqslant 0.06$, crystals exhibit a ferroelectric phase transition at T_C from a paraelectric phase with a space group $P6_322$ (PE phase) to a low-temperature ferroelectric phase with a $P6_3$ structure with doubled a and b axes (FE phase). Additionally, the temperature dependence of the dielectric constant ε' exhibits a peak at T_C. As x increases, T_C decreases substantially, and the peak at T_C becomes small. For $x \geqslant 0.07$, the peak is barely noticeable and becomes an anomaly at $T^* \approx 200$ K, indicating that the system possesses another state (FL state) below the T^*. The PE phase has been reported to possess two energetically competing soft modes at the M and K points. Electron diffraction (ED) experiments revealed that the superlattice reflections of the FE phase become diffuse scatterings originating from the M-point soft mode as the FE-FL boundary is approached. The K-point soft mode disappears in the FL state, whereas the M-point soft mode survives and fluctuates without condensation. Dark-field (DF) images revealed that the M-point soft mode exhibits coherent motion in nanodomains with sizes of approximately 10 nm in the FL state. The emergence of the FL state is ascribed to enhanced vibration of the AlO_4 tetrahedra resulting from the substitution of Sr, which has a smaller ionic radius than Ba.

DOI: 10.1103/PhysRevB.94.184106

I. INTRODUCTION

Condensation of a soft mode and the structural phase transition involved have been extensively studied with continuous efforts over the past decades. The most intensively studied ferroelectric materials, such as the perovskite-type oxides [1,2], have broadened our knowledge of these phenomena. Meanwhile, there has been increasing interest in the improper-type ferroelectrics, in which the polarization is only a secondary order parameter of the phase transition, since the multiferroic materials became highlighted. Research for new improper-type ferroelectrics and study on the structural phase transitions they exhibit are of great importance for further development of the ferroelectric materials.

The ferroelectrics $AEAl_2O_4$ (AE = Sr and Ba) belong to the large family of stuffed tridymite-type oxides [3–5]. $BaAl_2O_4$ is an improper-type ferroelectric, whereas $SrAl_2O_4$ is a proper-type ferroelectric [6]. At high temperatures, both compounds have an isomorphous crystal structure (PE phase, space group $P6_322$, $a_p = b_p \approx 5.2$ Å and $c_p \approx 8.6$ Å) comprising an AlO_4 network with shared vertices and six-membered cavities occupied by AE ions. The crystal structure of the ferroelectric phase (FE phase) depends on the AE ion; $BaAl_2O_4$ crystallizes in the $P6_3$ structure ($2a_p \times 2b_p \times c_p$) below $T_C = 400$–450 K [3,7,8], whereas $SrAl_2O_4$ adopts the $P2_1$ structure below 953 K [5]. For $SrAl_2O_4$, an intermediate $P6_3$ phase ($\sqrt{3}a_p \times \sqrt{3}b_p \times c_p$) exists in the temperature range of 953–1133 K [5,9].

In the structural phase transition of $BaAl_2O_4$, the M-point instability is the primary order parameter and corresponds to the M_2 soft mode [10]. As the M_2 mode is combined with the polar Γ_2 mode, the system enters into the ferroelectric transition. In the resultant $P6_3$ structure, the Ba ions displace along the c axis, resulting in a small polarization [8,10]. The M-point soft mode essentially corresponds to a so-called rigid unit mode (RUM) [11–13], which is correlated motion of the rigid AlO_4 tetrahedra. Because the RUM does not involve large distortion in each tetrahedron, relatively low-energy vibration is realized.

The RUM, which acts as the M-point soft mode, gives rise to the thermal diffuse scatterings observed at the M point in the electron diffraction (ED) patterns over a wide temperature range [14]. Our previous first-principles calculations [7] revealed the significant circular motion in the apical O(1) atoms, which connect the AlO_4 tetrahedra along the c axis, and vibration in the in-plane O(2) atoms for the M-point soft mode. Such thermal diffuse scatterings have also been observed in the $Ba_{1-x}Sr_xAl_2O_4$ solid solution with $x = 0.4$, which has the $P6_322$ parent structure at room temperature [15–17]. In the structural refinements for $x = 0.4$, this structural fluctuation is described as positional disorders in the individual atoms, with remarkable disorder in the apical O(1) atom [15]. Interestingly, diffuse scatterings have also been observed at the K point in the ED patterns [14–17]. According to the phonon calculations [7], $BaAl_2O_4$ possesses a soft mode with the RUM nature also at the K point, whose energy is nearly the same as that of the M-point soft mode. Below T_C, the M-point soft mode condenses, giving rise to the $P6_3$ low-temperature phase, and the K-point soft mode disappears.

We have recently investigated the crystal structure of $Ba_{1-x}Sr_xAl_2O_4$ system ($x = 0$–0.5) and found that it exhibits a "fluctuating" state (FL state), in which the M-point soft mode does not condense but survives and fluctuates down to low temperature, below $T_f \sim 200$ K for $x = 0.1$–0.5 [18]. The T_C is substantially suppressed by a small amount of Sr substitution and disappears at $x = 0.1$ [18]. Although the K-point soft mode disappears below T_f, the $P6_322$ crystal

*ishii@mtr.osakafu-u.ac.jp

structure is retained at temperatures down to 15 K [19]. In addition, the wave vector $\boldsymbol{q}$ of the diffuse scatterings at the M point is temperature dependent below T_f and deviates from the commensurate value $\boldsymbol{q} = (0,1/2,0)$ as the temperature decreases [18]. However, the behavior of the dielectric property near the border of this fluctuating state has been unclear.

Here we aimed to clarify the dielectric properties and the microstructures of the improper ferroelectric $Ba_{1-x}Sr_xAl_2O_4$ with $x \leqslant 0.1$. We present an anomaly near T_f in the dielectric constant, which is correlated with the disappearance of the K-point soft mode.

II. EXPERIMENT

Polycrystalline samples of $Ba_{1-x}Sr_xAl_2O_4$ ($x = 0$–0.1) were synthesized using a conventional solid-state reaction method. $BaCO_3$ (Kojundo Chemical, 3N), $SrCO_3$ (Kojundo Chemical, 3N), and Al_2O_3 (Kojundo Chemical, 4N) powders were mixed at a molar ratio of $1-x : x : 1$ and calcined at 1200° C for 10 h and 1300° C for 12 h in air with intermediate grinding. The obtained powder was uniaxially pressed into a pellet and then pressed again under hydrostatic pressure. The pellets were sintered at 1450° C and then cooled in a furnace. The obtained samples were stored in vacuum.

The synchrotron XRD experiments were conducted at the BL02B2 beamline at SPring-8 over a temperature range of 15–800 K. The incident x-ray beam was monochromatized to 25 keV using a Si (111) double crystal. T_C was defined as the temperature below which the superlattice reflection disappeared. The dielectric properties were measured at 2–400 K and 10 kHz using a pseudo four-probe method in a physical property measurement system (PPMS, Quantum Design). In these measurements, the dielectric losses, which were approximately 0.01, were sufficiently low. The ED experiments were performed at 90–300 K with a temperature interval of 10 K using a double-tilted liquid N_2 cooling holder in the JEM2100F and JEM-2010 TEM systems (JEOL, Japan). After reaching the desired temperature, all of the diffraction patterns were collected with a time interval of more than 30 min until no changes in the diffraction pattern were observed. Single crystals were used for the high-resolution transmission electron microscopy observation of $x = 0$. The single-crystal preparation method is described elsewhere [7].

III. RESULTS AND DISCUSSION

The powder XRD experiments revealed that all of the obtained samples were single-phase samples with a negligibly small amount of impurities. Figure 1(a) shows the synchrotron XRD patterns obtained at 100 K for $x = 0$–0.07. The Miller indices are based on the $P6_322$ parent phase. The superlattice reflections caused by doubling the cell parameters in the a and b axes were clearly seen for $x = 0$ and are marked by arrows, indicating that the sample crystallizes in the $P6_3$ superstructure. The superlattice reflections were observed at $T \leqslant 420$ K for $x = 0$. Our previous study shows that the T_C drastically decreases as x increases [19]. As x increases, the superlattice intensities are largely suppressed, and the full width at half maximum (FWHM) increases, as shown in Fig. 1(a).

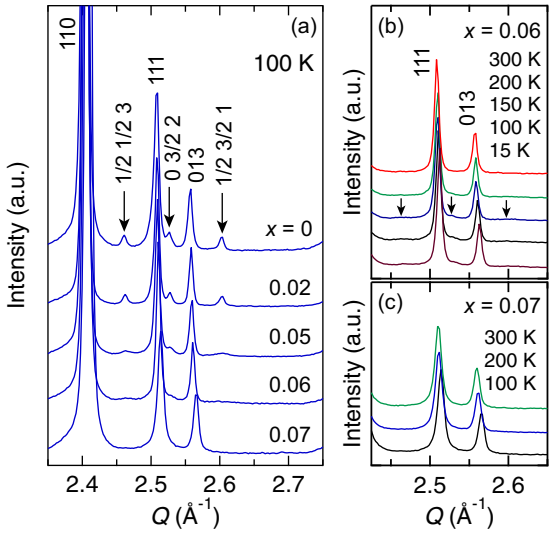

FIG. 1. (a) Synchrotron powder XRD patterns obtained at 100 K for $Ba_{1-x}Sr_xAl_2O_4$ ($x = 0$–0.07). The peaks were normalized using the 012 reflection of each pattern. The Miller indices are based on the $P6_322$ parent phase. The superlattice reflections are indicated by arrows. (b) and (c) show the diffraction patterns of $x = 0.06$ and $x = 0.07$, respectively, obtained at various temperatures.

This observation indicates that the Sr substitution suppresses the long-range correlation of the $P6_3$ superstructure. This result is in good agreement with a previous report [18]. For the $x = 0.06$ sample, broad peaks can be identified near the peak positions of the superlattice reflections. The temperature variations of the diffraction patterns for $x = 0.06$ and 0.07 are displayed in Figs. 1(b) and 1(c), respectively. For the $x = 0.06$ sample, broad peaks can be observed at $T \leqslant 150$ K, although they do not develop as sharp diffraction peaks, even at 15 K. The superlattice reflections are completely absent for the $x = 0.07$ sample, as shown in Fig. 1(c). The diffraction pattern for $x = 0.07$ is independent of temperature in the temperature range of 100–300 K. The absence of the superlattice reflections was also found for $x \geqslant 0.08$.

The dielectric constants ε' for these samples are displayed in Figs. 2(a) and 2(b) as a function of temperature. Prominent peaks were observed for the $x = 0.02$–0.05 samples and indicate the ferroelectric phase transitions. The onset of the peak is defined as T_C and indicated in Fig. 2. Although the values of ε' is increased at T_C for each composition, no divergence at T_C is found. This behavior is characteristic of improper ferroelectrics. A similar behavior was reported previously for $BaAl_2O_4$ polycrystalline samples [8]. No ferroelectric peaks are observed for $x = 0$ and 0.01 because the T_C values of these samples exceed 400 K. Additionally, both the T_C and the peak height decrease as x increases, which can be attributed to the broadening and suppression of the superlattice reflections of the $P6_3$ phase. For $x = 0.06$, a small peak can still be recognized in the ε'-T curve, indicating the formation of the FE phase, although the superlattice peaks are very broad. For the $x \geqslant 0.07$ samples, the ferroelectric peak disappears, corresponding to the disappearance of the superlattice reflections in the XRD data. Nevertheless, weak anomalies were observed near 200 K for $x \geqslant 0.07$; however,

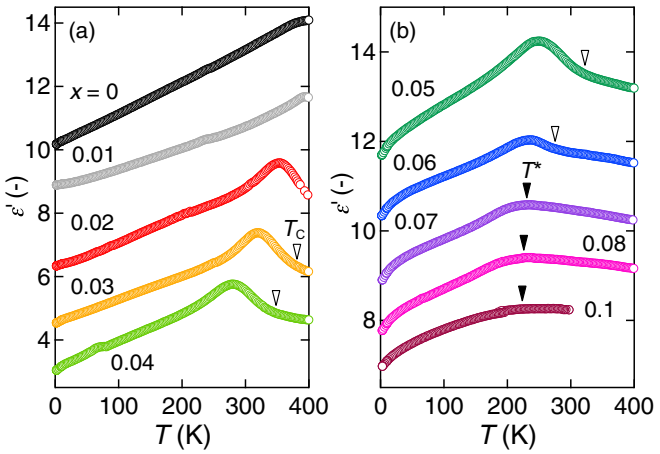

FIG. 2. Temperature dependence of the dielectric constant obtained at 10 kHz for $Ba_{1-x}Sr_xAl_2O_4$ with (a) $x = 0$–0.04 and (b) $x = 0.05$–0.1. The dielectric curves other than $x = 0$ and 0.05 are shifted parallel to the longitudinal direction for clarity. Open and closed triangles indicate T_C and T^*, respectively.

the XRD experiments revealed no structural phase transition at the anomaly. The slope of the ε' changes at the anomaly, which temperature is indicated by T^* in Fig. 2(b).

The T_C and T^* values obtained from the dielectric measurements are summarized in Fig. 3, together with the previously reported T_C [19], determined as the temperature at which the superlattice reflections appear in the synchrotron XRD experiments. For $x = 0.05$, the T_C obtained from Fig. 2 coincides well with the value determined from the XRD profiles. For $x \leqslant 0.02$, the T_C determined from the synchrotron XRD are on the extension of the fitted curve for the T_C determined from the dielectric data. For $x = 0.06$, a difference was observed between the T_C values determined from the dielectric measurements and the XRD data. This gap is

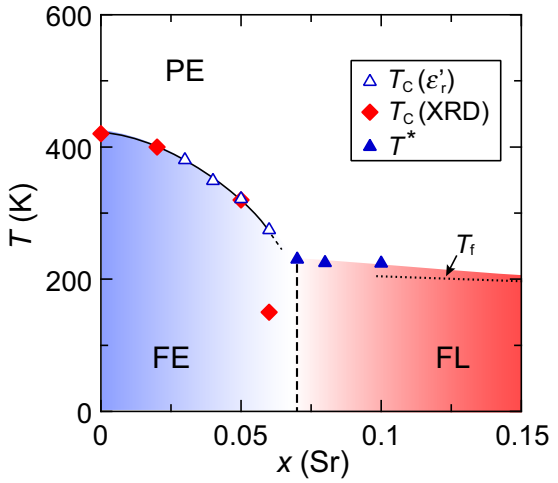

FIG. 3. Phase diagram of $Ba_{1-x}Sr_xAl_2O_4$. The previously reported T_C values [19] determined from the synchrotron XRD data are also plotted in the figure (red diamonds). The PE and FE phases indicate the paraelectric and ferroelectric phases, respectively. T_f denotes the temperature below which the K-point instability disappears [18]. The region below the T_f is indicated by the FL state.

probably attributable to the superlattice reflections of $x = 0.06$ being so broad that the T_C could not be determined accurately.

Notably, the T^* is located near the T_f line [18]. According to the previous study, two soft modes at the M and K points coexist above the T_f [18]. Although the latter mode disappears for temperatures below T_f, the former mode does not condense. That is, the M-point soft mode still exists at temperatures below T_f. Our structural analyses using a Rietveld method [19] and the ED technique [18] revealed that the crystal structures below and above T_f can be completely analyzed using a $P6_322$ symmetry. This result is also confirmed by the present XRD patterns shown in Fig. 1(c). The anomaly at the T^*, therefore, is ascribed to the disappearance of the K-point soft mode. The region below T_f and T^* is denoted by FL state in Fig. 3. On approaching the FL state, the superlattice reflections become smaller and broader, as shown in Fig. 1(a).

To clarify the mechanism for the emergence of the FL state, we performed microstructure observations using HRTEM and dark-field (DF) imaging techniques. Figure 4(a) displays the HRTEM image for $x = 0$ obtained at 300 K with a [001] incidence. The inset shows the corresponding diffraction pattern. The superlattice reflections caused by the $P6_3$ phase are clearly seen, as indicated by red circles. Meandering black lines are clearly observed in the HRTEM image, as indicated by arrows, and are identified as antiphase boundaries (APBs). The largest antiphase domain is approximately 60 nm wide. The meandering lines were also observed for $x = 0.05$ at 90 K, as shown in Fig. 4(b), obtained with a [001] incidence. The typical domain size for $x = 0.05$ is smaller than that for $x = 0$.

Figure 4(c) represents the typical DF image for $x = 0$ obtained at 300 K using a 1/2 1/2 2 superlattice reflection. A single domain covers the entire area of the crystal, and no defects, such as 180° twin walls or enantiomorphic domain walls, are observed. The inset shows the corresponding diffraction pattern obtained with a $[\bar{1}10]$ incidence. As shown in the inset, sharp superlattice reflections are observed at $(h + 1/2, k + 1/2, l)$ reciprocal positions.

The domain structure drastically changes as x increases. Figure 4(d) shows the DF image for $x = 0.05$ obtained at 100 K using a 1/2 1/2 2 superlattice reflection. Narrow and short stripes of several nanometers in width and approximately 100 nm in length are evident. Small speckles of several nanometers in length are also observed, as indicated by the broken circle. In the corresponding ED pattern shown in the inset of Fig. 4(d), weak streaks along [110] are observed, as indicated by red arrows. Because the white and black stripes are parallel to [001], they are likely responsible for the weak streaks observed in the ED pattern. In addition, the spot shapes of the superlattice reflections are slightly elongated along the [110] direction, which is in good agreement with the XRD result. The broadening of the superlattice reflections arises from the formation of the fine domain structure.

Figure 4 (e) shows the DF image for the $x = 0.06$ sample obtained at 100 K using a 1/2 1/2 2 superlattice reflection. Fine white and black speckles are clearly present. The strong streaks observed in the corresponding diffraction pattern are ascribed to the formation of these fine domains. The spot shapes of the superlattice reflections are further elongated along the [110] direction. According to the previous HRTEM experiments and fast Fourier transform analyses, the $P6_3$ crystal structure

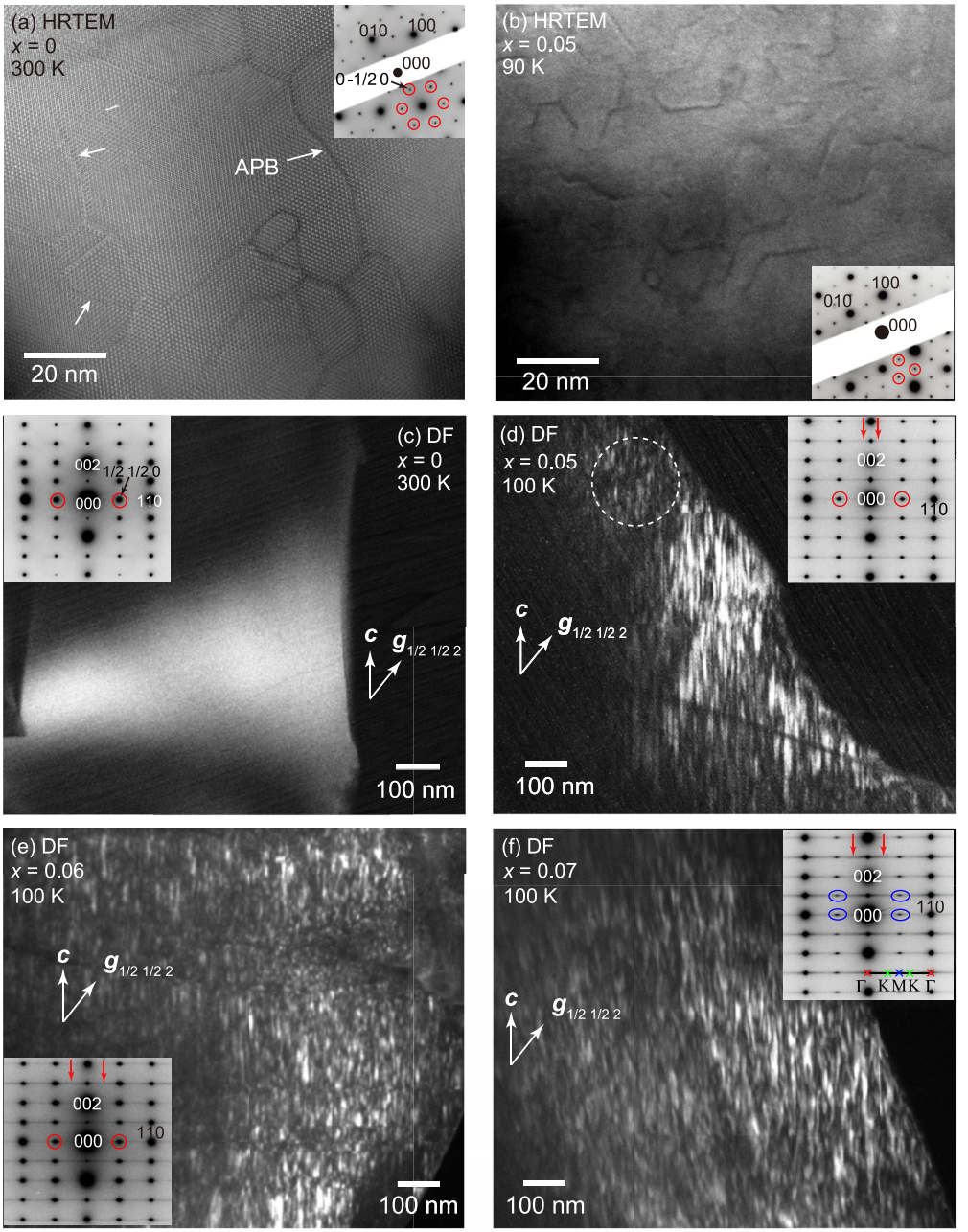

FIG. 4. HRTEM images of (a) $x = 0$ at 300 K and (b) $x = 0.05$ at 90 K obtained with a [001] incidence. DF images of (c) $x = 0$ at 300 K, (d) $x = 0.05$ at 100 K, (e) $x = 0.06$ at 100 K, and (f) $x = 0.07$ at 100 K using 1/2 1/2 2 superlattice reflections. For the images (c)–(f), the incidence is close to the $[\bar{1}10]$ direction. Insets show the corresponding diffraction patterns. The superlattice reflections arising from the FE phase are indicated by red circles with fractional indices. The diffuse scatterings at the M point are denoted by blue circles. The red arrows indicate the diffuse streaks caused by the fine domain structure.

reported for $BaAl_2O_4$ is not correct on the local scale [20]. Larsson *et al.* reported that the local symmetry is most likely reduced from $P6_3$ to orthorhombic or monoclinic in very small regions. The observed black speckles in Fig. 4(e) may stem not only from the difference in the structure factors between $\boldsymbol{g}$ and $-\boldsymbol{g}$ vectors but also the local disorder.

Similar white and black speckles were also observed in the DF image of the $x = 0.07$ sample below T_f, as shown in Fig. 4(f). However, because no superlattice reflections are observed in Fig. 1(c), the spots at the $(h + 1/2, k + 1/2, l)$ reciprocal positions (the M points) do not correspond to the superlattice reflections but, instead, reflect the diffuse scatterings from the M-point soft mode. In the corresponding ED pattern, the Γ, M, and K points are shown. The diffuse scatterings at the M point are indicated by blue circles. There are no diffuse scatterings at the K point, indicating the absence of the K-point soft mode. The spot at the (1/2, 1/2, 2) reciprocal position used for the DF image of $x = 0.07$ corresponds to the diffuse scatterings from the M-point soft mode. According to the previous report [18], the intensities

at the $(h + 1/2,\ k + 1/2,\ l)$ reciprocal positions remain temperature dependent below T_f. That is, the structural instability at the M point still exists in the FL state. Therefore, the white speckles observed for $x \geqslant 0.07$ are ascribed to the regions where the M-point soft mode has coherent motion.

Upon approaching the FE-FL boundary, the superlattice reflections become broader, as shown in Fig. 1(a), indicating that the long-range correlation of $P6_3$ is suppressed. This fact is in good agreement with the smaller FE domains observed for the $x = 0.05$ shown in Fig. 4(b). The substitution of Sr ions at Ba sites enables the AlO_4 tetrahedra to rotate or tilt more freely because Sr^{2+} ions are smaller than Ba^{2+} ions, thereby enhancing the motion of the RUMs. This process results in a decrease in T_C, and reduces the long-range correlation of the $P6_3$ superstructure. The reduced spatial correlation of the $P6_3$ superstructure leads to the formation of nanodomains. On the border of the FE-FL boundary, the short-range correlation of $P6_3$ becomes the M-point soft mode. In the FL state, the M-point soft mode is enhanced due to the high Sr concentration. Thus, the M-point soft mode cannot condense in the FL state and instead fluctuates with coherent motion down to low temperatures in nanodomains.

IV. CONCLUSIONS

The dielectric properties and microstructure of the improper ferroelectric $Ba_{1-x}Sr_xAl_2O_4$ ($x \leqslant 0.1$) were investigated. The PE phase possesses two independent soft modes at the M and K points. In the low-Sr-concentration region of $x \leqslant 0.06$, the M-point soft mode condenses at T_C, yielding the FE phase, and the K-point soft mode disappears. Substituting Sr ions at Ba sites substantially suppresses the T_C and weakens the spatial correlation of the $P6_3$ structure, leading to the formation of fine domain structures of $P6_3$. On the border of the FE phase near $x = 0.07$, the short-range correlation of the $P6_3$ structure becomes the M-point soft mode, and the FL state grows. At the PE-FL boundary, the dielectric constant exhibits an anomaly corresponding to the disappearance of the K-point soft mode, which is present in the PE phase. In the FL state, the K-point soft mode is absent, but coherent vibration of the M-point mode exists within nanodomains that are approximately 10 nm in size. This FL state is a unique feature of this system, and further investigations, including structure refinements using single crystals of $x \geqslant 0.07$, are needed to clarify the nature of this FL state.

ACKNOWLEDGMENTS

This work was partially supported by a Grant-in-Aid for Scientific Research from the Ministry of Education, Culture, Sports, Science and Technology of Japan (MEXT) of the Japan Society for the Promotion of Science (JSPS) and grants from The Murata Science Foundation. The synchrotron radiation experiments were performed at BL02B2 in SPring-8 with the approval of the Japan Synchrotron Radiation Research Institute (JASRI) (Proposal No. 2016A1349).

[1] R. E. Cohen, Nature (London) **358**, 136 (1996).
[2] D. Vanderbilt, Curr. Opin. Solid State Mater. Sci. **2**, 701 (1997).
[3] S.-Y. Huang, R. V. D. Mühll, J. Ravez, and M. Couzi, Ferroelectrics **159**, 127 (1994).
[4] U. Rodehorst, M. A. Carpenter, S. Marion, and C. M. B. Henderson, Mineral. Mag. **67**, 989 (2003).
[5] M. Avdeev, S. Yakovlev, A. A. Yaremchenko, and V. V. Kharton, J. Solid State Chem. **180**, 3535 (2007).
[6] J. M. Perez-Mato, R. L. Withers, A.-K. Larsson, D. Orobengoa, and Y. Liu, Phys. Rev. B **79**, 064111 (2009).
[7] Y. Ishii, S. Mori, Y. Nakahira, C. Moriyoshi, J. Park, B. G. Kim, H. Moriwake, H. Taniguchi, and Y. Kuroiwa, Phys. Rev. B **93**, 134108 (2016).
[8] S.-Y. Huang, R. V. D. Mühll, J. Ravez, J. P. Chaminade, P. Hagenmuller, and M. Couzi, J. Solid State Chem. **109**, 97 (1994).
[9] K. Fukuda and K. Fukushima, J. Solid State Chem. **178**, 2709 (2005).
[10] H. T. Stokes, C. Sadate, D. M. Hatch, L. L. Boyer, and M. J. Mehl, Phys. Rev. B **65**, 064105 (2002).
[11] M. T. Dove, V. Heine, and K. D. Hammonds, Mineral. Mag. **59**, 629 (1995).
[12] K. D. Hammonds, M. T. Dove, A. P. Giddy, V. Heine, and B. Winkler, Am. Mineralog. **81**, 1057 (1996).
[13] M. T. Dove, K. D. Hammonds, V. Heine, R. L. Withers, X. Xiao, and R. J. Kirkpatrick, Phys. Chem. Miner. **23**, 56 (1996).
[14] A. M. Abakumov, O. I. Lebedev, L. Nistor, G. V. Tendeloo, and S. Amelinckx, Phase Trans. **71**, 143 (2000).
[15] K. Fukuda, T. Iwata, and T. Orito, J. Solid State Chem. **178**, 3662 (2000).
[16] E. Tanaka, Y. Ishii, H. Tsukasaki, H. Taniguchi, and S. Mori, Jpn. J. Appl. Phys. **53**, 09PB01 (2014).
[17] S. Mori, Y. Ishii, E. Tanaka, H. Tsukasaki, and S. Kawaguchi, Jpn. J. Appl. Phys. **54**, 10NC02 (2015).
[18] Y. Ishii, H. Tsukasaki, E. Tanaka, and S. Mori, Sci. Rep. **6**, 19154 (2016).
[19] S. Kawaguchi, Y. Ishii, E. Tanaka, H. Tsuksaki, Y. Kubota, and S. Mori, Phys. Rev. B **94**, 054117 (2016).
[20] A.-K. Larsson, R. L. Withers, J. M. Perez-Mato, J. D. F. Gerald, P. J. Saines, B. J. Kennedy, and Y. Liu, J. Solid State Chem. **181**, 1816 (2008).